ELSEVIER

Chemical Physics 184 (1994) 335–346

Chemical Physics

Kinetics of multiphoton excitation and fragmentation of C_{60}

Peter Wurz [a], Keith R. Lykke [b]

[a] *Physikalisches Institut, Universität Bern, Sidlerstrasse 5, 3012 Bern, Switzerland*

[b] *Materials Science and Chemistry Divisions, Argonne National Laboratory, Argonne, IL 60439, USA*

Received 15 February 1994

Abstract

We report experimental and theoretical results on the kinetics of multiphoton excitation and fragmentation patterns due to UV-laser excitation of C_{60}. Multiphoton excitation of C_{60} is modeled including singlet and triplet states. Results show that a many-photon excitation event can have a low-order dependence on the laser fluence. In addition, we show why femtosecond excitation or nanosecond excitation with wavelengths shorter than ~215 nm can yield direct ionization without fragmentation or delayed ionization. The fragmentation is modeled by a total rate theory. Interpretation of the measured fragmentation data is in terms of sequential evaporation of C_2 units from the highly excited C_{60} and subsequent fragments. Larger C_n units may contribute ~5 to 10% to the fragmentation pattern.

1. Introduction

Since the first observation of a new class of carbon molecules [1] and the following identification of the special stability of one of them, namely C_{60} [2], many laboratories moved into this new and exciting field of research. Observations of photophysical processes are possible in C_{60} that cannot be studied for other molecules of comparable or even smaller size, taking advantage of the very rigid and highly symmetric molecular structure of this remarkable molecule [2]. The explanation of these photophysical processes has already helped the general understanding of the interaction of photons with large molecules [3–5] and promises to reveal more of its details. Precise knowledge of these ionization mechanisms is extremely important for the field of molecular mass spectrometry since the efficient ionization and detection of large molecules still pose a significant problem to the community [6,7].

We showed in a recent paper [5] that the absorption of several photons in the visible and ultraviolet spectral region by C_{60} leads to the formation of a highly internally excited parent molecule C_{60}^* using a 5 ns excitation pulse. Although only two to three photons are necessary for direct multiphoton ionization, the absorption of 10 to 20 photons is observed. The absorption of that many photons does not lead to ionization of the molecule because conversion from electronic to internal excitation is much faster than the absorption of additional photons, facilitated by the enormously high density of vibrational states in a molecule of this size [5].

Two major processes result from the high internal excitation of the molecule: fragmentation and delayed ionization. Both processes have macroscopic analogs, namely evaporation and thermionic electron emission from a hot medium. In our previous paper, we extensively dealt with thermionic electron emission from C_{60} and the fragmentation $C_{60} \rightarrow C_{58} + C_2$. We modeled this process with quasi-equilibrium theory [8] and determined the activation energy for this process to be ~5.6 eV. There are several reports in the literature for the

SSDI 0301-0104 (94)00087-Q

determination of the activation energy for this process. The first report of the activation energy for fragmentation of C_{60} is 4.6 ± 0.5 eV by Radi et al. [9]. The re-evaluation of these data by Klots gives a value of 5.9 ± 0.3 eV [10]. Sandler et al. found an activation energy 5.2 eV [11] by studying the kinetic energy release distributions from fragmentation of C_{60}. Later the same group reported an activation energy of 6.05 eV [12] because of improved measurements and more elaborate data analysis. A vacuum ultraviolet (VUV) single-photon ionization study yielded a range of 6.0–6.5 eV for the activation energy [13]. Most recently, a value of 7.1 ± 0.4 eV was found by analyzing time-resolved breakdown graphs of C_{60} [14].

Most of the theoretical values reported for the dissociation energy for C_{60} are much larger than the experimental numbers. Stanton [15] calculates a value of 11.8 eV for the dissociation energy from C_{60} to $C_{58} + C_2$. A recent calculation by Eckhoff and Scuseria [16] yields the same value. A detailed theoretical study of the dependence of the activation energy on the temperature of the molecule by a molecular dynamics simulation is given by Kim et al. [17]. These authors find that the activation energy drops from initially 8 eV for cold C_{60} (~ 1000 K) to less than 6 eV for hot C_{60} (~ 6000 K). Since the different experimental conditions in the preparation of C_{60}^+ give rise to different temperatures of the molecules and therefore different activation energies, the spread of the reported experimental values for the activation energy is not surprising.

In this paper, we study the kinetics of multiphoton excitation in C_{60}, and we look at the fragmentation behavior that invariably accompanies multiphoton ionization of C_{60} [18,19]. The first part of the paper will be devoted to modeling the important aspects of photon absorption into a multiple of energy levels. From these studies, we show why femtosecond excitation and nanosecond excitation with wavelengths shorter than 215 nm may yield direct ionization without fragmentation or delayed ionization. In addition, we show that these many-photon ionization events as mentioned above can have a very low-order fluence dependence.

In the second half of the paper, we will discuss the loss of fragments from C_{60}. Only even-numbered fragments are observed in the range from C_{58} down to C_{32} [4,18,19]. It is generally assumed that these fragments still have a cage structure similar to the parent molecule, C_{60}, with C_{32} the smallest stable cage; stable in respect to the observation time of time-of-flight instruments. Below C_{32}, cages are very unstable, and rings and chains are more favorable structures [20]. In our model, we assume a fragmentation process by successive loss of C_2 units, starting with the highly excited C_{60} molecule down to its smallest cage-like fragment, C_{32}. Many experimental results can be interpreted strongly in favor of fragmentation by loss of C_2 molecules rather than single C atoms. However, a definitive proof for that assumption is still missing. We present calculations of absolute rates for fragmentation, using a method introduced by Engelking [21,22]. The calculation of absolute rates allows for a better comparison with the experimental results than the rate constants obtained from the quasi-equilibrium theory.

2. Experimental

The instrument used for these experiments is a laser ionization mass spectrometer for molecular mass analysis. This instrument is identical to the one we used in our previous study [5]; a detailed description can be found in ref. [23]. The mass spectrometer is a linear time-of-flight (TOF) instrument of 120 cm length. The typical operating vacuum is 2×10^{-9} Torr. An effusive source generates a molecular beam of C_{60} in the ionization region of the mass spectrometer. The effusive source is a Ta cup (6.3 mm diameter, 8 mm long) with an aperture of 0.5 mm on the end directed to the laser beam. The Ta cup is resistively heated and the temperature is monitored with a chromel/alumel thermocouple. The Ta cup is filled with approximately 200 mg pure C_{60} (>99%), which is synthesized and purified in our laboratory according to published procedures [24–26]. The effusive source is operated at a temperature of ~ 800 K, corresponding to vapor pressure [27] of $\sim 5 \times 10^{-4}$ Torr in front of the aperture and $\sim 3 \times 10^{-7}$ Torr in the ionization volume. The ions are brought to their final kinetic energy with a two-stage acceleration field before they enter the field-free drift section. Ion detection is accomplished with a dual channel-plate assembly. The maximum mass resolution ($m/\Delta m$) of the instrument is approximately 1500 (fwhm at 720 amu) using a 5 ns ionization pulse. Data are recorded in a transient digitizer with a maximum time resolution of 5 ns or with a digital oscilloscope with

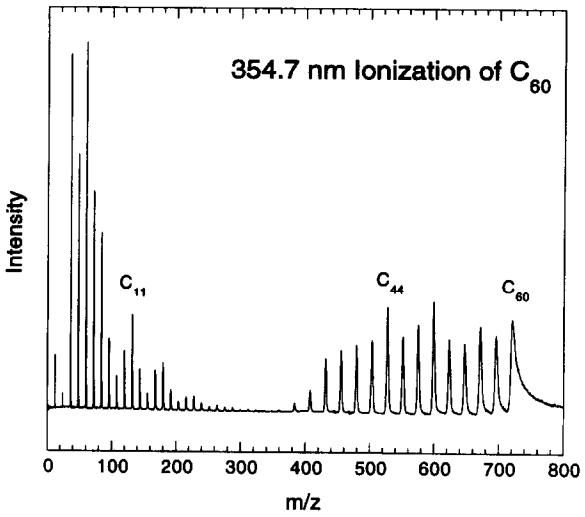

Fig. 1. time-of-flight mass spectrum of photoionization of C_{60} at $\lambda = 354.7$ nm.

2.5 ns time resolution. Further processing of the data is accomplished in a PC-based software system.

3. Experimental results

Fig. 1 shows a photoionization spectrum of C_{60} using 354.7 nm radiation from a Nd:YAG laser. This spectrum is very similar to any other spectrum obtained with multiphoton ionization of C_{60}. The main features are the high-mass, even-carbon-numbered fragments (fullerene fragments C_{58}–C_{32}, discussed here and earlier) and the low-mass fragments $< C_{32}$. The "magic numbers" for the low-mass fragments have been discussed in detail before. The most stable carbon molecular positive ions for this mass region are the C_n with $n = 4k + 3$, with $k = 2, 3, 4$ [1,18,28]. This is a consequence of the lower ionization potential of $4k + 3$ molecules (i.e., these molecules are easier to ionize) and the loss of C_3 units for these smaller C molecules. Recently there has been much experimental work [20,29] done on these low-mass C molecules showing that the very small molecules ($n < 6$) are strictly linear, the medium-mass molecules ($7 < n < 20$) change to monocycle and multicycle rings, and the larger species ($n > 30$) are fullerenes (closed cages). Fig. 2 is an expansion of the region between C_{13} and C_{36}. We see that there is a gap between C_{27} and C_{30}, as has been noticed previously. However, also noticeable above the noise are C_{28}, C_{29}, and C_{31}.

Fig. 3 is a collection of mass spectra obtained with three different laser fluences of 202 nm laser radiation. The top spectrum at low laser fluence shows no delayed ionization and no fragmentation, while the other two spectra taken at higher laser fluence demonstrate both of these processes. Whenever delayed ionization is observed, fragmentation is present and vice versa. This is what led us to propose in Ref. [5] that these two processes have similar precursors. From models of thermionic emission and RRKM modeling of fragmentation, we then proposed that this precursor is a superexcited state of C_{60}, mainly thermally excited to at least 50 eV of internal energy. Recently, Zhang and Stuke [30] have shown that laser radiation with wavelengths shorter than ~ 215 nm yields a transition from delayed ionization to direct ionization. They ascribe this transition to triplet–triplet interactions and claim that it is possible to observe delayed ionization without fragmentation or fragmentation without delayed ionization. We never observe one without the other. Fig. 4 is a blowup of Fig. 3B and shows how the enhanced sensitivity and mass resolution compared to Zhang and Stuke's allows us to observe the delayed ionization and fragmentation close to their fluence threshold. The inset ot the figure displays C_{60} and C_{58}, with the isotopic multiplet evident in the prompt ionization for C_{60}, but not evident in the broad C_{58} peak. Also evident in the figure is a very small peak due to C_{70} at the $< 10^{-3}$

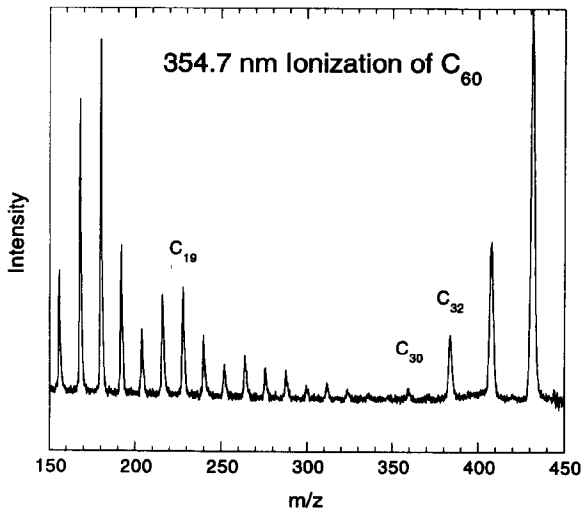

Fig. 2. Expansion of the mass spectrum shown in Fig. 1.

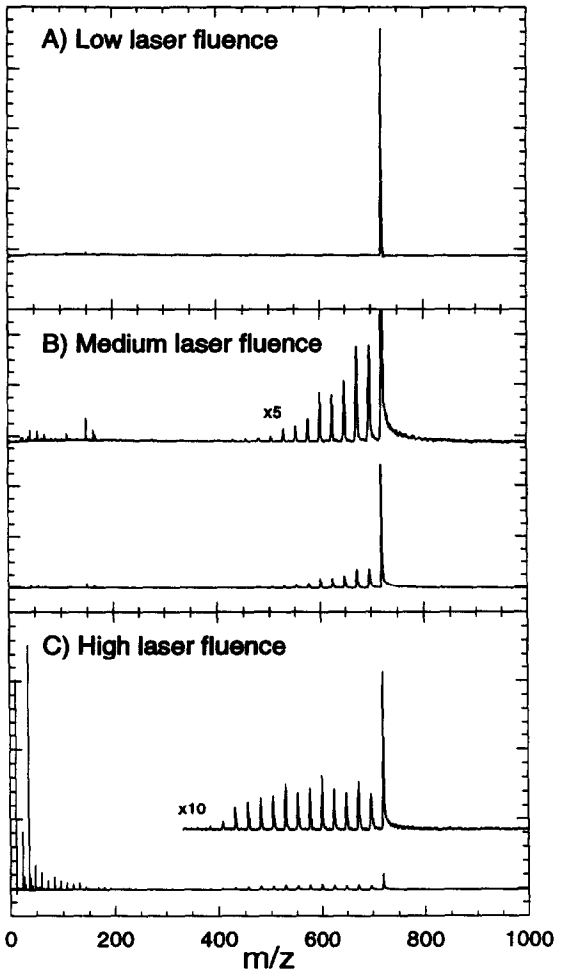

Fig. 3. Time-of-flight mass spectra of 202 nm laser ionization of C_{60}. The top spectrum is for low laser fluence, the middle spectrum is for medium laser fluence, and the bottom spectrum is for high laser fluence.

relative abundance to C_{60}. Although we will not discuss it here, C_{70} shows very similar behavior to C_{60} in terms of delayed ionization and fragmentation.

Fig. 5 shows that we can fit the delayed ionization tail from the data shown in Fig. 4 to a sum of two exponentials, with rate constants of $\sim 1.6\times10^{6}\,s^{-1}$ and $\sim 2\times10^{7}\,s^{-1}$. C_{60} is the peak at 27 μs, with the fragment peaks displaced to lower time (C_{58} at ~26.5 μs, C_{56} at ~26 μs, etc.). The fit is shown in the inset to the figure and from inspection, one can see that the sum of these two exponentials fits the data very well. Also evident in this figure are the delayed ionization tails on some of the fragments. We will not discuss the delayed ionization fitting in this paper since we have discussed it in detail previously [5]. Since the delayed ionization is very similar for wavelengths below and above 215 nm, we can be reasonably confident that the same photophysical processes are occurring throughout the wavelength interval measured. However, the addition of a prompt ionization signal below 215 nm needs some additional explanation.

4. Model of the multiphoton kinetics

We have modeled the multiphoton processes that are active in C_{60} and other fullerenes. Since we will be discussing some fluence-dependence data in our modeling of multiphoton excitation of C_{60}, we show in Fig. 6 the fluence-dependence data for 212.8 nm radiation of C_{60} (this is a reproduction of data from Ref. [5]). The important facts about this figure are:

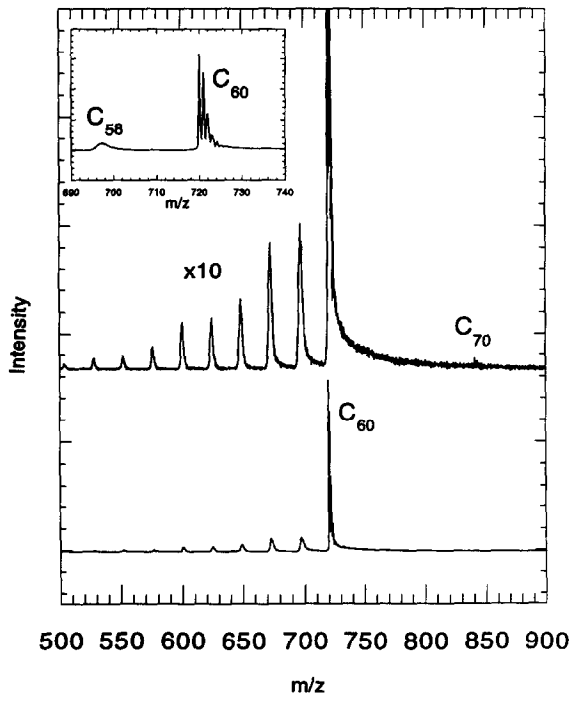

Fig. 4. Expansion of the middle spectrum from Fig. 3. Notice the high mass resolution that allows the different isotopes of C_{60} to be correctly identified (as shown in the inset to the figure). Also, notice the fragmentation peaks and the delayed ionization signal (the "tail" on the C_{60} peak).

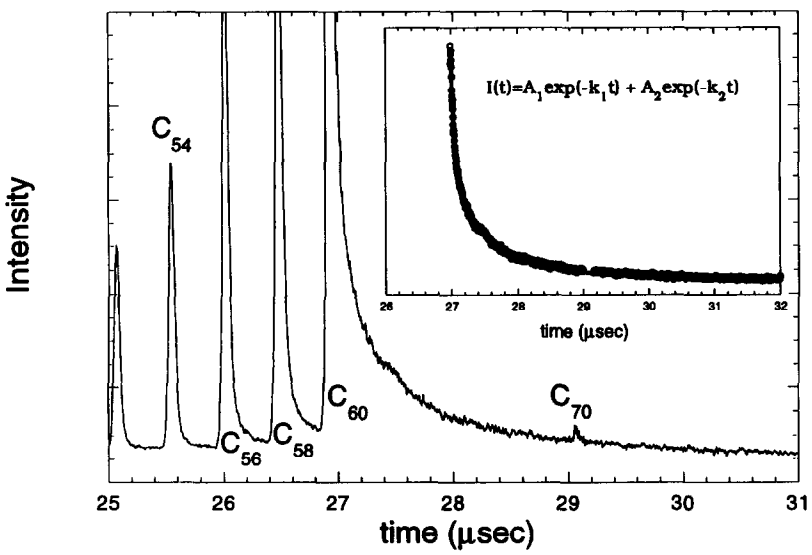

Fig. 5. Time-of-flight spectrum for C_{60} ionization with 202 nm laser radiation. The inset shows a fit to the delayed ion signal from C_{60} in the range from 27 to 32 μs.

(1) The C_{60} prompt ion signal has a very low fluence order ($1 < n < 2$).

(2) The delayed ionization fluence dependence and the fragments' fluence dependence are greater than the prompt ionization fluence dependence and are approximately equal to each other.

(3) The signals saturate at some fluence level. The saturation fluence depends on fragment size, such that the saturating fluence increases as the size of the fragment shrinks. This will be discussed in more detail later.

Shown in Fig. 7 is a schematic diagram of the energy levels we use to model the kinetics for multiphoton

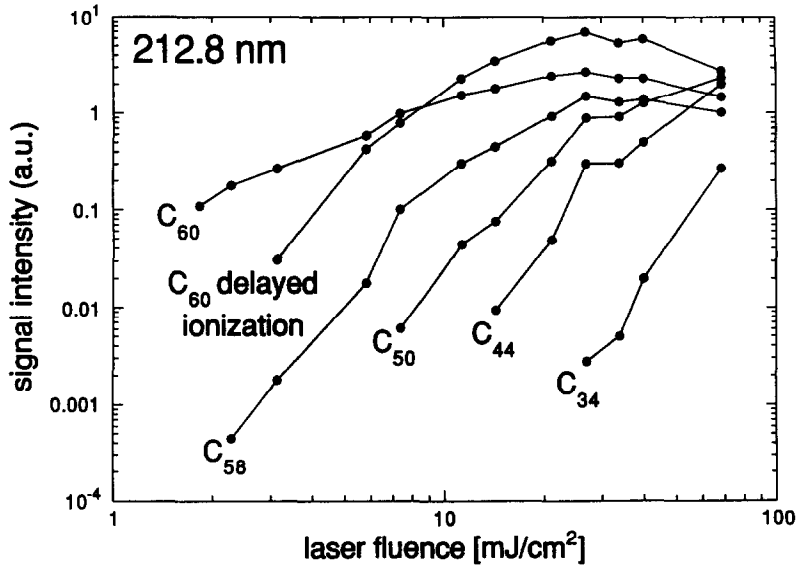

Fig. 6. Laser fluence dependence of C_{60} ions and some representative fragment ions for 212.8 nm photo-excitation of C_{60}. The signal intensities are integrated over the peak areas in the mass spectra. This integral is split into two components, a prompt and a delayed contribution, labeled "C_{60}" and "C_{60} delayed ionization", respectively.

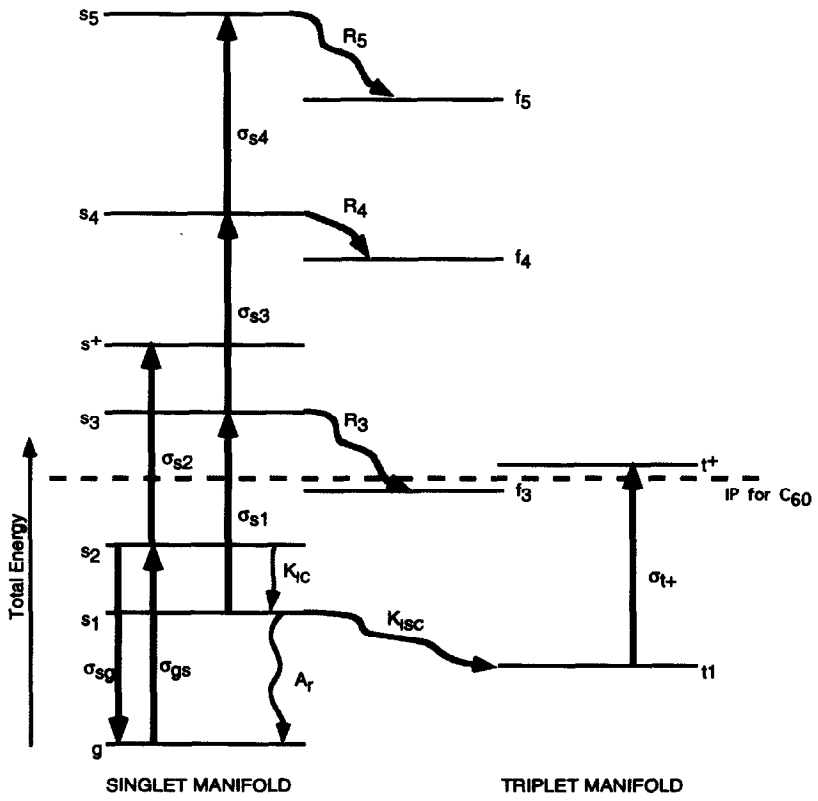

Fig. 7. Energy levels and photo-excitation process used to model the excitation of C_{60}. See text for details.

absorption in C_{60} (which also applies to other fullerenes). The model includes a ground state g, a singlet manifold $s_1 \ldots s_5$, a singlet ion state s_+ (this is actually a doublet state of the ion, but is from ionization through the singlet state manifold and yields prompt ionization), a triplet manifold t_1, t_2, a triplet ion state t_+ (also

Table 1
Parameters used in modeling C_{60} multiphoton excitation

$\sigma_{sg} = \sigma_{gs} = 10^{-16}$ cm^2	absorption cross section from ground state
$\sigma_{s1} = 10^{-16}$ cm^2	absorption cross section from first excited singlet state
$\sigma_{s2} = 10^{-16}$ cm^2	absorption cross section from second excited singlet state
$\sigma_{s3} = 10^{-15}$ cm^2	absorption cross section from third excited singlet state
$\sigma_{s4} = 10^{-14}$ cm^2	absorption cross section from fourth excited singlet state
$\sigma_{t+} = 5 \times 10^{-17}$ cm^2	absorption cross section from lowest triplet state
$K_{IC} = 10^{12}$ s^{-1}	internal conversion rate
$K_{ISC} = 10^{9}$ s^{-1}	intersystem crossing rate
$R_3 = 10^{7}$ s^{-1}	destruction (dissociation and ionization) rate for s_3; (this corresponds to ~45 eV internal energy in C_{60}, see Fig. 16 in Ref. [5])
$R_4 = 10^{8}$ s^{-1}	destruction (dissociation and ionization) rate for s_4 (~55 eV internal energy)
$R_5 = 10^{9}$ s^{-1}	destruction (dissociation and ionization) rate for s_5 (~65 eV internal energy)
$A_r = 10^{8}$ s^{-1}	fluorescence rate to ground singlet state
$I(t)$ = laser intensity =	$A \exp\{-\frac{1}{2}[(t-t_0)/\text{width}]^2\}$

prompt ionization but through the triplet manifold), and states that will decay with time f_3 to f_5 which comprise fragmentation and delayed ionization. The energy (vertical axis) actually represents total energy (electronic, vibrational, and rotational) in the C_{60} molecule. In fact, the excited singlet states represent internally excited states of some of the low-lying electronic singlet states in C_{60}.

For the population of the ground state, we have

$$\frac{d}{dt} g(t) = -g(t)\sigma_{gs} I(t) + s_2(t)\sigma_{sg} I(t) + A_r s_1(t) . \tag{1a}$$

For excitation of the singlet manifold, we get

$$\frac{d}{dt} s_1(t) = -s_1(t)[\sigma_{s1} I(t) + A_r + K_{ISC}] + s_2(t) K_{IC} ,$$

$$\frac{d}{dt} s_2(t) = g(t)\sigma_{gs} I(t) - s_2(t)[\sigma_{s2} I(t) + \sigma_{sg} I(t) + K_{IC}] ,$$

$$\frac{d}{dt} s_3(t) = s_1(t)\sigma_{s1} I(t) - s_3(t)[\sigma_{s3} I(t) + R_3] ,$$

$$\frac{d}{dt} s_4(t) = I(t)[s_3(t)\sigma_{s3} - s_4(t)\sigma_{s4}] - s_4(t) R_4 ,$$

$$\frac{d}{dt} s_5(t) = s_4(t)\sigma_{s4} I(t) - s_5(t) R_5 . \tag{1b}$$

Ionization from the singlet manifold is given by

$$\frac{d}{dt} s_+(t) = s_2 \sigma_{s2} I(t) . \tag{1c}$$

For excitation of the tiplet states, we have

$$\frac{d}{dt} t_1(t) = s_1(t) K_{ISC} - t_1(t)\sigma_{t+} I(t) . \tag{1d}$$

Ionization out of the triplet manifold

$$\frac{d}{dt} t_+(t) = t_1(t)\sigma_{t+} I(t) \tag{1e}$$

and the population of the states that will undergo decay

$$\frac{d}{dt} f_3(t) = s_3(t) R_3 ,$$

$$\frac{d}{dt} f_4(t) = s_4(t) R_4 ,$$

$$\frac{d}{dt} f_5(t) = s_5(t) R_5 . \tag{1f}$$

The model necessarily neglects many of the excited states and limits the number of accessible levels to twelve to allow numerical solution of the differential equations with *Mathematica* on a Macintosh Ilsi computer. As stated above, we know from our earlier study that we must include up to 50 eV of excitation to obtain a realistic description to explain the observed phenomena (>8 photons for 200 nm radiation). The present model, although simple, allows for a detailed understanding of some of the details of the important photophysical effects involved in the kinetics of multiphoton excitation of C_{60}.

The molecules start out in the ground electronic state with a vibrational distribution given by the temperature of the effusive source. The laser pumps molecules up to an excited singlet state with a cross section σ_{sg} that has been measured for the condensed phase (see Table 1 for a listing of the cross sections and rates used in the model). These excited species may then either relax (E–V relaxation given by K_{ic}, internal conversion) into excited vibrational states in other singlet levels, decay to the triplet state manifold, or absorb more photons to undergo further excitation. The cross sections for absorption up the multiphoton ladder will increase because of the plethora of energy levels (huge density of states). These excited species will then keep absorbing photons until the rate constant for decay (either thermionic emission or fragmentation) increases to the point that the molecule decays. Molecules that decay into the triplet state manifold may then either decay back to the singlet states (very long time constant, $\sim 10^5\ s^{-1}$) or may absorb more photons. If the photon energy is large enough, the molecule will be one-photon ionized. If the photon energy is too small and the molecule cannot be one-photon ionized, they will absorb more photons (much like the singlet state manifold) and be further excited until they decay via thermionic emission, fragmentation, or photon emission.

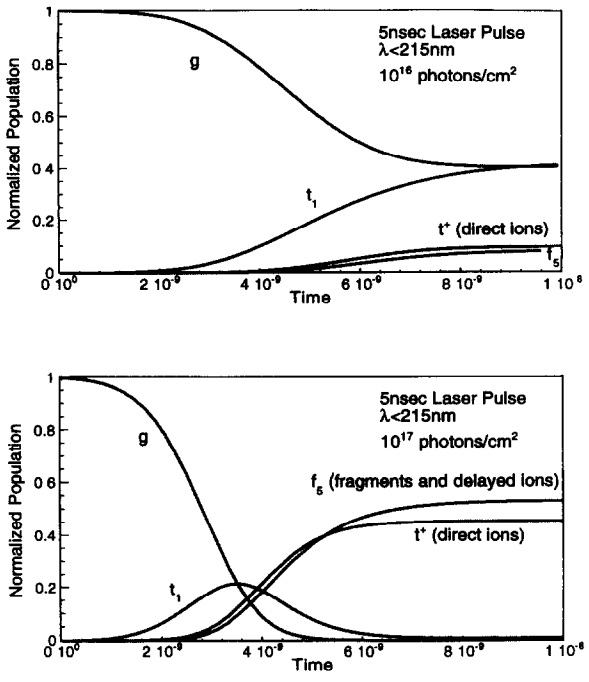

Fig. 8 Plots of the population versus time for two different laser fluences. The laser pulse is a Gaussian with a maximum at 5×10^{-9} s. See text for details.

We have taken literature values where they are known and have estimated the remaining cross sections. The values used are given in Table 1, along with the other parameters used in our model. Fig. 8 displays representative results for two laser fluences with 5 ns excitation and laser radiation of $\lambda < 215$ nm, where ionization from the triplet levels is possible. At low laser fluence, the molecules are not excited out of the ground singlet state. At higher fluence (top panel in Fig. 8, fluence $= 10^{16}$ photons/cm^2 ~ 10 mJ/cm^2 at 200 nm), the molecules are excited into the ground triplet state (via excited singlet states) and may then ionize by absorbing one more (<215 nm) photon. This is shown as t_+ in Fig. 8. If the laser wavelength is >215 nm, the next photon will not ionize the molecule, and multiphoton absorption will ensue. In addition, the presence of "f_5" (fragments and delayed ions) shows that multiphoton excitation has occurred at this fluence level. At even higher fluences (bottom panel of Fig. 8, fluence $= 10^{17}$ photons/cm^2 ~ 100 mJ/cm^2 at 200 nm), more "f_5" (fragments and delayed ions) than "t_+" (direct ionization through the triplet state) species are formed because the up-pumping rate through the singlet manifold beats the $\sim 10^9$ s^{-1} rate for intersystem crossing. This is even more pronounced at higher fluences.

Fig. 9 shows the computed fluence dependence for multiphoton excitation with wavelengths <215 nm. As can readily be identified from this simple model, the ionization through the triplet state has a fluence dependence between 1 and 2 at low fluence and then saturates at a higher fluence, which fits the experimental data (prompt ionization) very well (see Fig. 6). In addition, the data for the state labeled "decayed state" (f_5 state in Fig. 7, the state that will either yield delayed ionization or fragmentation) has a lower than fourth order dependence (the number of photons needed to be absorbed to yield f_5), which it should have if all cross sections were identical.

Fig. 10 shows another calculation of the fluence dependence of the various levels for 500 fs laser pulse duration. These results are markedly different than the ns pulse duration in that the sub-picosecond pulse enables ionization via the singlet manifold (prompt ionization) that is even the dominant pathway in the excitation scheme. In this case, the very intense subpicosecond radiation allows the multiphoton excitation of electronic states by overwhelming the internal conversion rates (here we use 10^{12} s^{-1} for the internal conversion rate). This demonstrates that femtosecond excitation of C_{60} (and other molecules) will allow frag-

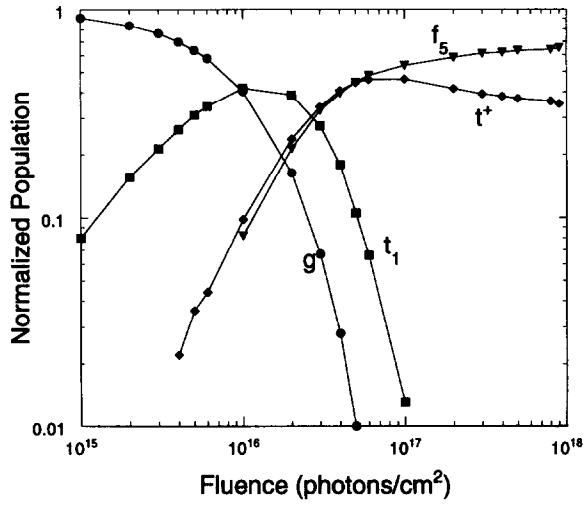

Fig. 9. Population versus fluence for 5 ns laser radiation and $\lambda < 215$ nm.

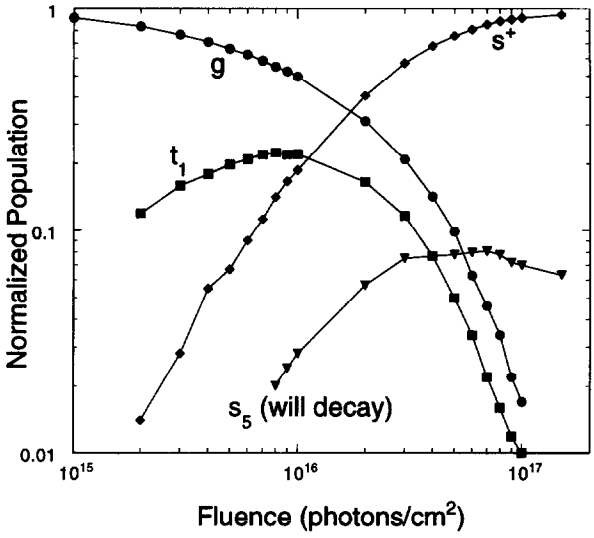

Fig. 10. Population versus fluence for 500 fs laser radiation. There is no significant t_+ shown because the short time scales preclude the excitation into the triplet manifold.

mentation-free ionization. In addition, no delayed ionization should be observed at these fluence levels. However, at higher fluences, fragmentation and delayed ionization (shown here as the "highly excited state s_5") will emerge. But, if either one appears, the other should be present and detectable with sensitive mass spectrometers. The simple model used allows for a good qualitative understanding of all of the experimental findings.

5. Model of the fragmentation process

The high internal energies should also explain the observed fragmentation spectra of laser-excited C_{60}. In the last paper, we showed that the process $C_{60}^* \rightarrow C_{58} + C_2$ can be modeled by unimolecular decay of a C_{60}^* molecule excited to ~50 eV internal energy. In the following, we show that the entire fragmentation pattern evolves from the superexcited molecule.

We shall analyze our mass spectra by assuming that the observed fragmentation pattern of C_{60} results from sequential fragmentation processes of the following form:

$$(C_{60})^* \xrightarrow{\Gamma_{58}} (C_{58})^* + C_2\,,$$

$$\vdots$$

$$(C_{2n})^* \xrightarrow{\Gamma_{2n-2}} (C_{2n-2})^* + C_2\,,$$

$$\vdots$$

$$(C_{34})^* \xrightarrow{\Gamma_{32}} (C_{32})^* + C_2\,, \qquad (2)$$

with Γ_i the total rate of fragmentation. Higher order processes, like loss of fragments larger than C_2 are not considered in the current theoretical treatment, although there are experimental [18] and theoretical [31] indications for the loss of C_n units up to C_8 in photo fragmentation. This will be discussed below. For the internal density of states, $N_i(E)$, of a cluster consisting of i atoms we use the formula given by Kassel [32]:

$$N_i(E) = E^{s_i - 1}\left((s_i - 1)! \prod_j^{s_1} (h\nu_j)\right)^{-1}, \qquad (3)$$

with s_i the number of internal modes of the cluster. The molecular structure and thus the vibrational frequencies are known only for C_{60} but not for the fragments. Therefore, we have to use an average frequency, $\nu = 1050$ cm^{-1} rather than sets of ν_j, to describe C_{60} and all the fragments. For the theoretical modeling of the fragmentation processes (Eq. (2)) we follow the treatment given by Engelking [21,22]. This approach to quasi-equilibrium-theory gives absolute rates rather than rate constants, which makes it much easier to compare the results with the measured data from the mass spectrometer. The total rate Γ_i for the dissociation is

$$\Gamma_i = \nu^3 (s-1) \frac{8\pi m_i g_i S_i (E_i - E_i^0)^{s-2}}{E_i^{s-1}}, \qquad (4)$$

where $s = s_{i+2}$, g_i is the remaining channel degeneracy, m_i is the reduced mass, S_i the geometrical cross section assuming a cage structure, E_i^0 is the activation energy and E_i the total internal energy for a cluster of size i. In the sequence of fragmentation the total internal energy of a fragment cluster of size i as obtained from its predecessor fragment is given by

$$E_i = E_{i+2} - \langle E_{i+2} \rangle - E_{i+2}^0\,, \qquad (5)$$

where the average kinetic energy release is given as

Table 2
Results from the calculation for initial energies of the parent C_{60} molecule 55, 45, 40 and 35 eV

Cluster size	E_i^0 (eV)	E_i (eV)	$\langle E_i \rangle$ (eV)	Γ_i (au)	Signal (au)	E_i (eV)	$\langle E_i \rangle$ (eV)	Γ_i (au)	Signal (au)
60	5.6	55.0	0.57	8.09(9)	1.60(8)	45	0.46	1.23(8)	1.03(8)
58	5.15	48.8	0.52	7.95(9)	1.38(8)	38.9	0.40	6.43(7)	5.85(7)
56	4.72	43.2	0.48	7.78(9)	1.73(8)	33.4	0.36	2.88(7)	3.55(7)
54	4.31	37.9	0.43	7.64(9)	1.34(8)	28.3	0.31	1.06(7)	1.82(7)
52	3.92	33.2	0.39	7.51(9)	1.38(8)	23.7	0.27	2.92(6)	7.67(6)
50	3.56	28.9	0.35	7.31(9)	1.95(8)	19.5	0.22	5.22(5)	2.39(6)
48	3.21	25.0	0.32	7.17(9)	1.38(8)	15.7	0.18	4.95(4)	4.72(5)
46	2.88	21.5	0.28	7.06(9)	1.09(8)	12.3	0.14	1630	4.78(4)
44	2.57	18.3	0.25	6.93(9)	1.30(8)	9.31	0.11	7.72	1620
42	2.28	15.5	0.22	6.84(9)	9.16(7)				
40	2.01	13.0	0.19	6.77(9)	7.51(7)				
38	1.76	10.8	0.17	6.70(9)	6.32(7)				
36	1.52	8.84	0.14	6.65(9)	5.44(7)				
34	1.31	7.18	0.12	6.63(9)	2.38(7)				
32	1.11	5.74	0.10	6.62(9)	5.36(6)				
60	5.6	40	0.40	6.33(6)	1.07(7)	35	0.34	1.26(5)	2.14(5)
58	5.15	34	0.36	1.79(6)	4.54(6)	29.1	0.29	1.25(4)	1.14(5)
56	4.72	28.5	0.30	3.46(5)	1.44(6)	23.6	0.23	513	1.20(4)
54	4.31	23.5	0.25	3.91(4)	3.07(5)	18.7	0.19	4.88	508
52	3.92	18.9	0.20	1870	3.72(4)	14.2	0.14		
50	3.56	14.8	0.16	20	1840	10.1	0.092		
48	3.21	11.1	0.12			6.46	0.047		
46	2.88	7.77	0.075						
44	2.57	4.81	0.036						
42									

$$\langle E_i \rangle = 2(E - E_i^0)/(s-1)\ . \qquad (6)$$

The fragmentation will continue to be observed until the total internal energy of a fragment is too small to give an appreciable signal in the measuring interval.

The results of the calculation described above are given in Table 2 for four different internal energies of the parent C_{60} molecule. To obtain the activation energies for the fragment clusters, we fit the absolute rates at 55 eV internal energy to the experimental spectrum taken at 130 mJ/cm^2. In our earlier paper [5], we concluded that under these experimental conditions the internal energy of the parent molecule will be around 50 eV. The energy of 55 eV was the lowest where it was possible to reproduce the whole set of measurements satisfactorily, that is, the absolute numbers as well as the individual fragment distributions. As can be seen in Table 2, the sequential fragmentation continues until enough of the initial excitation is used up. A comparison of the calculated signal values for the cluster fragments with measurements taken at 266 nm for different laser fluences is depicted in Fig. 11. Good agreement is found between the calculations and the measurements. In particular, the absolute yields are reproduced satisfactorily by the calculation. The worst agreement between experiment and theory is found at 45 eV internal energy, where we are off by a factor of 2 from the measured numbers. The energy range where fragmentation is observable in our experiment, 35 to 55 eV, agrees well with calculations we published earlier. The kinetic energy release derived from Eq. (6) seems a bit too high compared to measured values, which are around 0.4 eV [9,11,12]. This could result from the different experimental conditions of our experiment. However, the kinetic energy release has only a minor effect on the outcome of the calculation since most of the energy loss is used for breaking the molecular bonds.

Since no structural details of the fragment clusters are incorporated into the theory, special stability of some fragments is not reproduced by the theoretical calculations. In the short time scale of a multi-photon

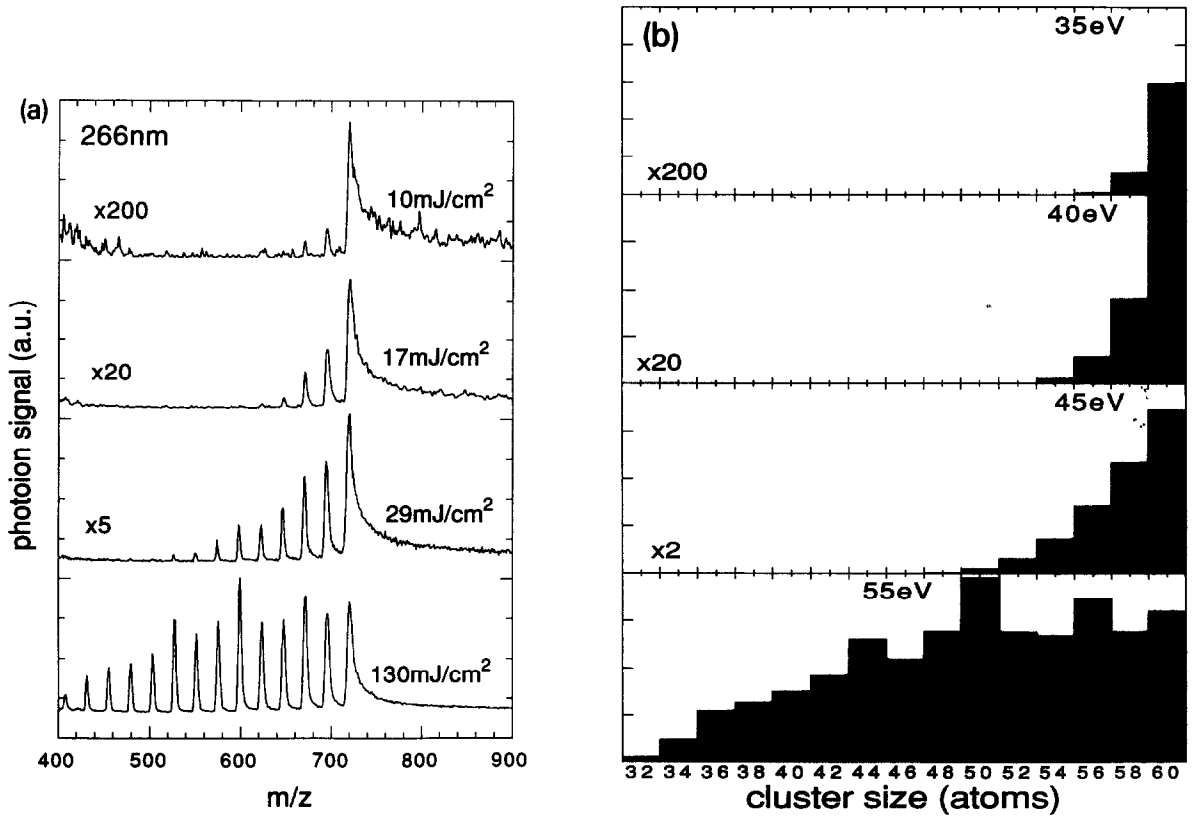

Fig. 11. Comparison of experimental photofragmentation spectra with the calculation of the fragmentation. Fragmentation is caused by a 266 nm pulsed laser (≈5 ns) at fluences of 10, 17, 29 and 130 mJ/cm². For details on the calculation see text.

experiment, the fragments are perhaps not even the proposed closed-shell structures since the time for annealing and assuming these more stable, closed, molecular structures may be too short. Evaporation could proceed from the rim of this structure, therefore the somewhat low activation energies we find for dissociation of the fragments could be explained. As already mentioned, the fragmentation by loss of larger C_n fragments than C_2 is not taken into account in our calculation, which would add to the yield of smaller size fragments. Because our calculation consistently underestimates the fragment yield by a small amount, a fragmentation channel by loss of large C_n fragments seems possible and could be of the order of 5 to 10% of the C_2 loss channel. Experimental indications for the loss of C_n units up to C_8 in photofragmentation have been reported [18,33]. In addition, it is still unclear if the fragmentation consists of C_2 loss or the sequential loss of two C atoms [34–36]. That is, does the C_{60} dissociate into a C_2 molecule and a C_{58} fragment, or does the dissociation proceed by loss of two C atoms sequentially? The former pathway will be lower in energy, but there may be constraints on the loss of a C_2 species from fullerenes. The conjecture that C_2 comes from C_{60} was made on the basis of the observation of only even-numbered fullerenes. It is possible that the C_{60} species dissociates into C_{59} that is very unstable with the internal energy left in it from the parent C_{60}, and undergoes extremely rapid dissociation into the much more stable even-numbered fullerene. Although some experiments have detected either C-atoms by resonantly-enhanced multiphoton excitation [35,36] or C_2 Swan-band emission in a microwave plasma of C_{60} [37], the nascent distribution of small neutral fragments has never been verified for C_{60} dissociation.

This experiment detects only positive ions from photodissociation. We have previously shown that the neutral fragment distribution is very similar to the ion fragment distribution [4]. The C_{60} molecules will fragment in the neutral "ladder" as well as in the ionic

ladder. It may be possible that for $\lambda > 300$ nm, most, if not all, of the fragment ions detected are generated from delayed ionization (thermionic emission) of neutral fragment molecules.

6. Conclusions

We have modeled multiphoton excitation of C_{60} to show that a many-photon excitation event can have a low-order dependence on the laser fluence. We have also shown why femtosecond excitation or nanosecond excitation with wavelengths shorter than ≈ 215 nm can yield direct ionization without the observation of fragmentation or delayed ionization. In addition, we showed that the fragmentation behavior can be understood in terms of sequential evaporation of C_2 fragments from the excited parent molecule as we proposed earlier [5]. This result contributes to the understanding of the processes involved that are encountered when attempting ionization of large molecules by multiphoton absorption. For large organic or even biomolecules, which do not have the special stability of C_{60}, the question was raised if they can by ionized at all by multiphoton or single-photon ionization [7]. The answer to this question is affirmative if one is able to keep the internal energy in the parent small enough during ionization so the molecule is stable during the analysis time of the instrument.

Acknowledgement

This work was supported by the U.S. Department of Energy, BES-Materials Sciences, under Contract W-31-109-ENG-38.

References

[1] E.A. Rohlfing, D.M. Cox and A. Kaldor, J. Chem. Phys. 81 (1984) 3322.
[2] H.W. Kroto, J.R. Heath, S.C. O'Brien, R.F. Curl and R.E. Smalley, Nature, 318 (1985) 162.
[3] P. Wurz and K.R. Lykke, J. Chem. Phys. 95 (1991) 7008.
[4] K.R. Lykke and P. Wurz, J. Phys. Chem. 95 (1992) 3191.
[5] P. Wurz and K.R. Lykke, J. Phys. Chem. 96 (1992) 10129.
[6] E.W. Schlag, J. Grotemeyer and R.D. Levine, Chem. Phys. Letters 190 (1992) 521.
[7] E.W. Schlag and R.D. Levine, J. Phys. Chem. 96 (1992) 10608.
[8] W. Forst, Theory of unimolecular reactions (Academic Press, New York, 1973).
[9] P.P. Radi, M. Hsu, M.E. Rincon, P.R. Kemper and M.T. Bowers, Chem. Phys. Letters 174 (1990) 223.
[10] C.E. Klots, Z. Physik. D 21 (1991) 335.
[11] P. Sandler, C. Lifshitz and C.E. Klots, Chem. Phys. Letters 200 (1992) 445.
[12] P. Sandler, T. Peres, G. Weissman and C. Lifshitz, Ber. Bunsenges. Physik. Chem. 96 (1992) 1195.
[13] R.K. Yoo, B. Ruscic and J. Berkowitz, J. Chem. Phys. 96 (1991) 911.
[14] M. Foltin, M. Lezius, P. Scheier and T.D. Mark, J. Chem. Phys. 98 (1993) 9624.
[15] R.E. Stanton, J. Phys. Chem. 96 (1992) 111.
[16] W.C. Eckhoff and G.E. Scuseria, Chem. Phys. Letters (1993), submitted for publication.
[17] E. Kim, Y.H. Lee and J.Y. Lee, Chem. Phys. Letters (1993) submitted for publication.
[18] S.C. O'Brien, J.R. Heath, R.F. Curl and R.E. Smalley, J. Chem. Phys. 88 (1988) 220.
[19] P. Wurz, K.R. Lykke, M.J. Pellin and D.M. Gruen, J. Appl. Phys. 70 (1991) 6647.
[20] G. von Helden, M.-T. Hsu, P.R. Kemper and M.T. Bowers, J. Chem. Phys. 95 (1991) 3835.
[21] P.C. Engelking, J. Chem. Phys. 85 (1986) 3103.
[22] P.C. Engelking, J. Chem. Phys. 87 (1987) 936.
[23] J.E. Hunt, K.R. Lykke and M.J. Pellin, Methods and mechanisms for producing ions from large molecules (Plenum Press, New York, 1990).
[24] W. Krätschmer, L.D. Lamb, K. Fostiropoulos and D.R. Huffman, Nature 347 (1990) 354.
[25] D.H. Parker, P. Wurz, K. Chatterjee, K.R. Lykke, J.E. Hunt, M.J. Pellin, J.C. Hemminger, D.M. Gruen and L.M. Stock, J. Am. Chem. Soc. 113 (1991) 7499.
[26] K. Chatterjee, D.H. Parker, P. Wurz, K.R. Lykke, D.M. Gruen and L.M. Stock, J. Org. Chem. 57 (1992) 3253.
[27] J. Abrefah, D.R. Olander, M. Balooch and W.J. Siekhaus, Appl. Phys. Letters 60 (1992) 1313.
[28] M.E. Geusic, M.F. Jarrold, T.J. McIlrath, R.R. Freeman and W.L. Brown, J. Chem. Phys. 86 (1987) 3862.
[29] J.M. Hunter, J.L. Fye and M.F. Jarrold, J. Chem. Phys. 99 (1993) 1785.
[30] Y. Zhang and M. Stuke, Phys. Rev. Letters 70 (1993) 3231.
[31] R.L. DeMuro, D.A. Jelski and T.F. George, J. Phys. Chem. 96 (1992) 10603.
[32] L.S. Kassel, J. Phys. Chem. 32 (1928) 225.
[33] P.P. Radi, T.L. Bunn, P.R. Kemper, M.E. Molchan and M.T. Bowers, J. Chem. Phys. 88 (1988) 2809.
[34] P. Hvelplund, L.H. Andersen, H.K. Haugen, J. Lindhard, D.C. Lorents, R. Malhotra and R. Ruoff, Phys. Rev. Letters 69 (1992) 1915.
[35] K.R. Lykke, P. Wurz, D.H. Parker and M.J. Pellin, Appl. Opt. 32 (1993) 857.
[36] D. Ding, R.N. Compton, R.E. Haufler and C.E. Klots, J. Phys. Chem. 97 (1993) 2500.
[37] D.M. Gruen, S. Liu, A.R. Krauss and X. Pan, J. Appl. Phys. 75 (1994) 1758.